

# The influence of multiple ionization thresholds on harmonic generation: Ar<sup>+</sup>

A. C. Brown and H. W. van der Hart  
Centre for Theoretical Atomic, Molecular and Optical Physics,  
Queen's University Belfast, Belfast, BT7 1NN, UK.

(Dated:)

We apply time-dependent  $R$ -matrix theory to investigate harmonic generation from ground state Ar<sup>+</sup> with  $M = 0$  at a wavelength of 390-nm. Contributions associated with the different  $3s^23p^4$  ionization thresholds are assessed, including the interference between these. The dominant contribution originates from the second ionization threshold,  $3s^23p^4\ ^1D$ . Changes to the harmonic yields arising from the higher  $3s3p^5$  thresholds are also assessed. We further confirm that Ar<sup>+</sup> has a higher harmonic yield than He for the same laser pulse, despite having a higher ionization threshold.

PACS numbers: 32.80.Rm, 31.15.A-, 42.65.Ky

## I. INTRODUCTION

Harmonic generation (HG) has been at the centre of atomic and molecular physics for over 20 years [1]. Not only is it the means of producing the ultrashort laser pulses which drive attosecond physics [2], but it has been adopted as an important measurement tool for some of the most fundamental physical atomic and molecular processes. HG has facilitated imaging molecular dynamics [3], obtaining detailed information about molecular orbitals [4] and has been employed to highlight the importance of electron correlation and multielectron dynamics in a variety of systems on ultrashort timescales [5–7].

Generally, HG is described in terms of a three-step model [8]: a laser field causes tunnel ionization of an electron, which is subsequently accelerated in the field. As the electric field changes direction, the electron is driven back towards its parent ion, and can be recaptured, emitting a high-energy photon. A semiclassical model of this process has proven highly successful in explaining experimental phenomena, particularly in noble-gas atoms [9].

The three-step model describes the main physics leading to HG, but the model cannot be applied directly to all atomic or molecular systems. It assumes that tunnel ionization leaves the residual ion in the ground state. This is appropriate for noble gas atoms, but may not be so for systems in which the residual ionic state lies close to other ionic states. Examples of such systems are primarily found in molecules such as N<sub>2</sub>. It is less appreciated that they can also be found in atomic systems, eg. Ar<sup>+</sup>. For these systems, electron-emission channels associated with different ionic states contribute to HG, and interference between these channels can be of significance. Since HG occurs within a laser field cycle, this interference provides information about ultrafast dynamics. To develop understanding of how this information can be extracted, accurate theoretical data is of great benefit. To obtain such data, it is imperative to apply theoretical methods capable of including multiple channels associated with different thresholds and the interactions between these channels: recent studies on the Cooper minimum in Ar have shown that the inclusion of multichannel effects can alter the harmonic yield by as much as two orders of

TABLE I: Energies of the five ionization thresholds of Ar<sup>+</sup> included in the present work with respect to the Ar<sup>2+</sup> ground state, and compared to literature values [14].

Configuration	Term	Energy (Lit.)	Energy (TDRM)
		eV	eV
$3s^23p^4$	$^3P$	0.00	0.00
	$^1D$	1.67	2.04
	$^1S$	4.06	3.85
$3s3p^5$	$^3P^o$	14.10	17.04
	$^1P^o$	17.79	24.83

magnitude [10].

We have recently developed capability within time-dependent  $R$ -matrix theory (TDRM) [11] to determine harmonic spectra for general multielectron atoms [7, 12]. TDRM is well-suited to study ultrafast multielectron dynamics, as demonstrated in a study of C<sup>+</sup> [13], and multichannel interferences in HG, as evidenced in a study of resonant enhancement of the 5th harmonic in Ar [7]. In order to study the interplay of multiple channels associated with low-lying thresholds, we apply TDRM to investigate HG from Ar<sup>+</sup> in a  $4 \times 10^{14}$  Wcm<sup>-2</sup>, 390-nm laser field. This intensity/wavelength regime can lead to significant non-perturbative changes in the atomic structure. Therefore, perturbative methods are not suitable for addressing an ion in these fields, even though the interaction can be characterised as a multiphoton process. Given the small energy gap between the relevant thresholds, we would expect that the general multichannel effects seen for 390-nm would still be important at 800-nm, even though the fine detail may differ.

Ar<sup>+</sup> is an ion well-suited to investigations on multiple thresholds: the lowest three ionization thresholds,  $3s^23p^4\ ^3P$ ,  $^1D$  and  $^1S$ , are separated from each other by about 2 eV (Tab. I). We can also investigate the effects of higher-lying thresholds by including the  $3s3p^5$  thresholds. Ar<sup>+</sup> thus allows the investigation of interference effects arising from the interplay between channels associated with well separated, as well as closely spaced, thresholds.

The harmonic response of Ar<sup>+</sup> to intense laser light is

also of relevance to experiment. The highest harmonics (up to 250 eV) generated by irradiation of Ar by intense laser light have been assigned to the response of  $\text{Ar}^+$  [15, 16]. A full picture of HG at high intensities should therefore include ionized species. Recent photoionization experiments and calculations also provide detailed information on resonances that may affect HG in  $\text{Ar}^+$  [17].

## II. THEORY

The TDRM approach is a non-perturbative, *ab initio* approach to describe multielectron atoms in short, intense light pulses. Full details of the method can be found in [11]. By propagating the solution of the time-dependent Schrödinger equation on a discrete time mesh of step size  $\Delta t$ , we can express its solution,  $\Psi_{t_{q+1}}$ , at time  $t_{q+1}$  in terms of the solution at the previous time step  $t_q$ :

$$(H_m - E)\Psi_{t_{q+1}} = -(H_m + E)\Psi_{t_q}. \quad (1)$$

Here,  $H_m$  is the Hamiltonian at the midpoint of the time interval, and it contains both the non-relativistic field-free atomic Hamiltonian and the laser interaction term. The laser field is assumed to be linearly polarized and spatially homogeneous and is described by the dipole approximation in the length form [18]. The imaginary energy,  $E$ , is defined as  $2i/\Delta t$ .

TDRM theory makes use of the  $R$ -matrix partition of configuration space. Within an inner region close to the nucleus, full account is taken of all electron-electron interactions. Outside of this region, exchange interactions between an ejected electron and those remaining close to the atomic core can be neglected, and the ejected electron moves only in the long-range multipole potential of the residual ion and the laser field.

We evaluate Eq. (1) at the boundary of this inner region,  $a_{\text{in}}$ , as a matrix equation [11]:

$$\mathbf{F}(a_{\text{in}}) = \mathbf{R}(a_{\text{in}})\bar{\mathbf{F}}(a_{\text{in}}) + \mathbf{T}(a_{\text{in}}), \quad (2)$$

in which the wavefunction,  $\mathbf{F}$ , at the boundary is expressed in terms of its derivative,  $\bar{\mathbf{F}}$ , and an inhomogeneous vector,  $\mathbf{T}$ , which arises from the right hand side of Eq. (1). The matrix  $\mathbf{R}$  connects the inner and outer region wavefunction at the boundary,  $a_{\text{in}}$ .

Given an inner region wavefunction,  $\mathbf{R}$  and  $\mathbf{T}$  are evaluated at the boundary, and propagated outwards in space to an outer region limit at which it can be assumed that the wavefunction has vanished. There, the wavefunction,  $F$ , can be set to zero and propagated inwards to  $a_{\text{in}}$ . Once  $F$  is determined at every boundary point, the full wavefunction can be extracted from the  $R$ -matrix equations. We can then iterate the procedure using Eq. (1).

The light radiated by an oscillating dipole is proportional to its acceleration [19, 20]. It is also possible to express the harmonic spectrum in terms of the dipole velocity or dipole operators [21–24]. For He, the different expressions have been shown to be both self-consistent

within TDRM, and consistent with the spectrum obtained by the HELIUM approach [12, 25]. We show only dipole length spectra here. We have verified that they are consistent with those based on the dipole velocity form.

The harmonic response of a single atom can be evaluated via the expectation value of the dipole operator:

$$\mathbf{d}(t) \propto \langle \Psi(t) | \mathbf{z} | \Psi(t) \rangle, \quad (3)$$

where  $\mathbf{z}$  is the total position operator along the laser polarization axis. The harmonic spectrum is then proportional to the square of the modulus of the Fourier transform of  $\mathbf{d}(t)$ ,  $|\mathbf{d}(\omega)|^2$ . We note that this is a non-relativistic approximation to the HG process. Inclusion of relativistic effects, such as spin-orbit coupling, would lead to the population of  $M = 1$  levels, and this is the subject of ongoing investigation.

## III. COMPUTATIONAL SETUP

In  $R$ -matrix theory,  $\text{Ar}^+$  is described as a state of  $\text{Ar}^{2+}$  plus an additional electron. To describe  $\text{Ar}^{2+}$ , we use a set of Hartree-Fock  $\{1s, 2s, 2p, 3s, 3p\}$  orbitals, obtained for the  $\text{Ar}^{2+}$  ground state [26]. We obtain the  $3s^2 3p^4$  and  $3s 3p^5$  eigenstates of  $\text{Ar}^{2+}$  from configuration-interaction calculations comprising  $3s^2 3p^4$ ,  $3s 3p^5$  and  $3p^6$ . No pseudo-orbitals are included, since such orbitals may lead to spectra influenced by unphysical resonances. A consequence of this basis-set restriction is that the energies of the  $\text{Ar}^{2+}$  thresholds differ by 0.2 and 0.4 eV from experiment for the  $3s^2 3p^4$  states and 3 and 7 eV for the  $3s 3p^5$  states (Tab. I). To assess interference effects, we employ several  $\text{Ar}^+$  models. The full  $\text{Ar}^+$  model contains all five  $\text{Ar}^{2+}$  thresholds. In the three-state model, only the  $3s^2 3p^4$  states of  $\text{Ar}^{2+}$  are retained. We also use  $\text{Ar}^+$  models in which only a single state or a pair of states from the  $3s^2 3p^4$  configuration is retained. In these latter models, both  $3s 3p^5$  states are always included.

The inner region has a radius of 15 a.u. which suffices to contain the residual  $\text{Ar}^{2+}$  ion. The outer region radius is 600 a.u. The set of continuum orbitals is built from 60  $B$ -splines for each angular momentum of the continuum electron. The  $\text{Ar}^+$  basis contains all allowed combinations of  $\text{Ar}^{2+}$  states and the set of continuum orbitals up to a total angular momentum  $L_{\text{max}} = 19$ . Convergence testing was carried out up to  $L_{\text{max}} = 23$ . The outer region is divided into sectors of 2 a.u. each containing 35  $B$ -splines of order 9 per channel. The time step in the wavefunction propagation is 0.1 a.u. We use 390-nm laser pulses, consisting of a 3 cycle  $\sin^2$  ramp-on followed by 2 cycles at peak intensity,  $4 \times 10^{14}$  W/cm<sup>2</sup>, and a 3 cycle  $\sin^2$  ramp-off. The initial state is the  $\text{Ar}^+$  ground state with total magnetic quantum number  $M = 0$ , which would be the dominant non-relativistic  $\text{Ar}^+$  ground state level following strong-field ionization of Ar at 390-nm.

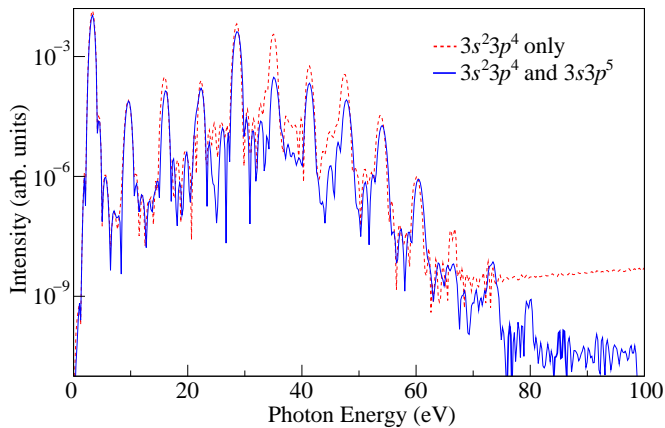


FIG. 1: (Color online) Harmonic spectrum of  $\text{Ar}^+$  produced by an 8-cycle  $4 \times 10^{14} \text{ Wcm}^{-2}$  laser pulse at 390-nm, as obtained by the three-state model (dotted, red line) and by the five-state model (solid, blue line).

#### IV. RESULTS

Figure 1 shows the harmonic spectra produced from the full and the three-state model of  $\text{Ar}^+$ . The three-step model [8] suggests a harmonic cut-off of 46 eV. Even though the three-step model may not apply at 390-nm, the harmonic spectra are not inconsistent with this value.

As shown in Fig. 1, inclusion of the  $3s3p^5$  thresholds has a noticeable effect on the yields for the 11th to the 15th harmonic, which are reduced by up to an order of magnitude. These harmonics coincide with the range of energies associated with the Rydberg series converging onto the  $3s3p^5$  thresholds. We can thus ascribe the differences between the two spectra as arising from the reaction of multiple electrons to the laser field. Rydberg series converging onto  $3s3p^5$  effectively describe the excitation of a  $3s$  electron, while the main contribution to the full harmonic spectrum involves the emission of a  $3p$  electron. This competition is similar to the one observed for HG in Ar [7]. However, the present study employs a longer wavelength and involves a five-photon gap between the  $3s^2 3p^4$  and  $3s3p^5$  thresholds.

The main focus of the present study is interference between channels associated with the three low-lying  $3s^2 3p^4$  thresholds. We have therefore calculated harmonic spectra using  $\text{Ar}^+$  models in which only selected  $3s^2 3p^4$  thresholds are included.

Figure 2 compares the harmonic spectra obtained by summing contributions of the individual  $3s^2 3p^4$   $^1D$  and  $^1S$  models, the individual  $3s^2 2p^4$   $^3P$ ,  $^1D$  and  $^1S$  models and the spectrum from the full model. The individual  $3s^2 3p^4$  models retain both  $3s3p^5$  thresholds. The spectrum is largely dominated by the  $^1D$  model, while the  $^3P$  model does not contribute significantly, especially in the cutoff region, as demonstrated by the small difference between the two summed spectra. The largest difference is seen for the 7th harmonic for which the  $^3P$  model

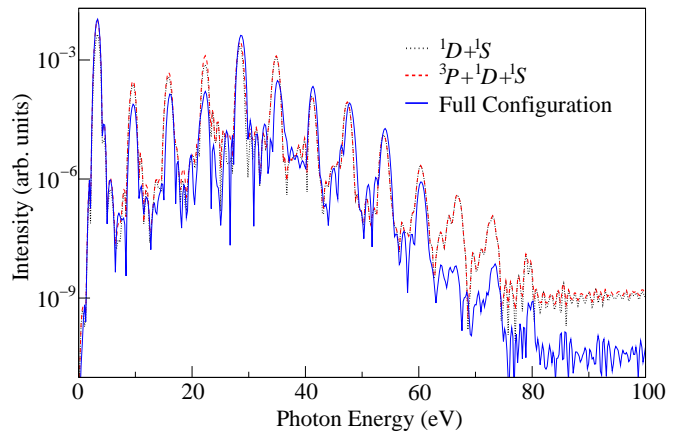


FIG. 2: (Color online)  $\text{Ar}^+$  harmonic spectrum produced by an 8-cycle,  $4 \times 10^{14} \text{ Wcm}^{-2}$  laser pulse at 390-nm as calculated by summing contributions of the individual  $3s^2 3p^4$   $^1D$  and  $^1S$  models (dotted, black line), the individual  $3s^2 2p^4$   $^3P$ ,  $^1D$  and  $^1S$  models (dashed red line) and from the full model (solid, blue line). All calculations include both  $3s3p^5$  thresholds.

contributes 41%. In terms of the three-step mechanism, this suggests that tunnel ionization leaving  $\text{Ar}^{2+}$  in the ground state does not significantly contribute to HG. In the three-step model for  $\text{Ar}^+$ , the first step should consider tunnel ionization leaving  $\text{Ar}^{2+}$  in an excited state.

Figure 2 shows that interference between channels associated with different  $3s^2 3p^4$  thresholds must be accounted for. The comparison between the summed spectra and the full model shows differences for the 3rd -7th harmonic and the 11th harmonic by as much as an order of magnitude, noticeable shifts in the energy of the 13th and 15th harmonics and reductions by two orders of magnitude for the 21st and 23rd harmonics. The accurate determination of  $\text{Ar}^+$  harmonic yields thus requires calculations including all  $3s^2 3p^4$  channels simultaneously.

To assess the interferences, we have performed calculations in which pairs of  $3s^2 3p^4$  thresholds of  $\text{Ar}^{2+}$  are retained. Of particular interest are the spectra in which we retain (a)  $3s^2 3p^4$   $^3P$  and  $^1D$  and (b)  $3s^2 3p^4$   $^3P$  and  $^1S$ . As shown in Fig. 3, the  $(^3P, ^1D)$  model provides a spectrum with harmonic peaks within 15% of the full model up to the 15th harmonic, apart from the 11th with a difference of 30%; the 17th and 19th peaks differ by 25%. Channels associated with the  $^3P$  and the  $^1D$  thresholds are hence the most important channels for HG. The improvement over the individual-state models (Fig. 2) shows that channels associated with the  $^3P$  threshold are important to HG beyond the  $^3P$  threshold, even though their direct contribution to these harmonics is relatively minor.

Addition of the harmonic spectra obtained from the  $(^3P, ^1D)$  and the  $(^3P, ^1S)$  model shows poor agreement for harmonics below the  $\text{Ar}^+$  ionization threshold as the Rydberg series leading up to the  $^3P$  threshold contributes twice. However, beyond this threshold, the agreement with the full model is very good, with harmonic peaks

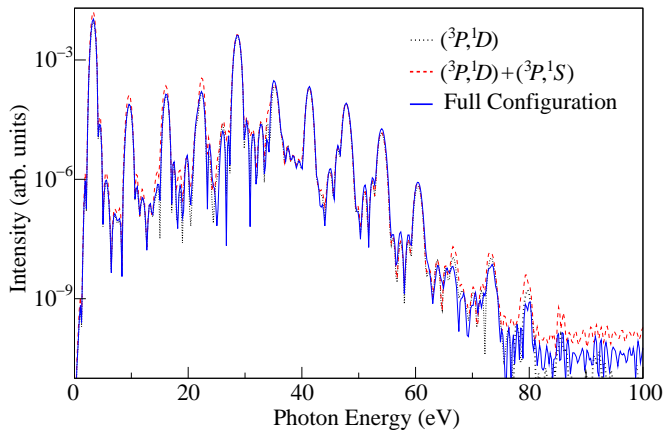


FIG. 3: (Color online)  $\text{Ar}^+$  harmonic spectrum produced by an 8-cycle  $4 \times 10^{14} \text{ Wcm}^{-2}$  laser pulse at 390-nm as obtained by the  $(^3P, ^1D)$  model (dotted, black line), by summing the spectra obtained by the  $(^3P, ^1D)$  model and the  $(^3P, ^1S)$  model (dashed, red line) and by the full model (solid, blue line).

differing by up to only 6% for the 9th to the 19th, apart from differences of 15% and 19% for the 11th and 17th harmonics. This comparison again indicates that HG due to channels associated with the  $^3P$  threshold primarily occurs below the ionization threshold. Above this threshold, HG from these channels is negligible.

The importance of the  $^3P$  threshold for an accurate harmonic spectrum can be understood by considering the atomic structure. The first step within the three-step model is emission of a single electron. For an accurate emission rate, the atomic structure up to the threshold must be described well. Inclusion of the  $^3P$  threshold is necessary to account for the Rydberg series leading up to the first ionization threshold. This series also affects the position of low-lying states such as  $3s3p^6$  and of low-lying members of Rydberg series leading up to other thresholds. Therefore, when HG originates from an excited threshold, atomic structure associated with the lower thresholds must still be accounted for.

Finally, we compare the efficiency of HG in  $\text{Ar}^+$  with that of other atoms.  $\text{Ar}^+$  has a slightly higher ionization potential, 27.6 eV, than He, 24.6 eV. On the other hand,  $\text{Ar}^+$  is a larger ion, and may therefore provide a greater harmonic response [15]. We also consider the  $\text{Ne}^+$  ion as it also is an ionized noble-gas atom, but with a substantially higher ionization potential, 40.96 eV.

Figure 4 shows the harmonic spectrum of  $\text{Ar}^+$ , He and  $\text{Ne}^+$  for the laser pulse used throughout. For He, we use the 6P-model described in our earlier work [12], whereas for  $\text{Ne}^+$  we include the three  $2s^22p^4$  and the two  $2s2p^5$  thresholds with the  $\text{Ne}^{2+}$  states generated following a similar procedure as outlined above for  $\text{Ar}^{2+}$ . Figure 4 shows expected behaviour for  $\text{Ne}^+$  and its higher ionization potential, with a harmonic yield several orders of magnitude smaller than that of He and  $\text{Ar}^+$ . However, the figure also shows that, apart from the 13th and 15th

harmonics, the harmonic yield from  $\text{Ar}^+$  is consistently higher than that from He, despite its larger ionization potential. Thus  $\text{Ar}^+$  is indeed an efficient ion for HG.

## V. CONCLUSION

We have applied TDRM theory to determine harmonic yields for ground-state  $\text{Ar}^+$  with  $M = 0$  and assess in detail the role of the various closely spaced ionization thresholds. The dominant contribution to the harmonic yield is associated with the first excited threshold instead of the lowest ionization threshold. This lowest threshold must still be accounted for, as it affects the atomic structure leading up to excited thresholds. The  $3s3p^5$  thresholds affect the harmonic yield significantly less, but need to be taken into account for harmonics with energies close to these thresholds. Overall, the harmonic yield for  $\text{Ar}^+$  is generally larger than the yield for He, even though  $\text{Ar}^+$  has a larger ionization potential.

In our discussion of the HG process we have frequently made reference to the three-step model, even though it may not be applicable this wavelength/intensity regime. However, the present calculation demonstrates that interaction between different channels is important for an accurate description of HG. Since the energy separation between the  $^3P$  and  $^1D$  thresholds is comparable to 800-nm photon energies we would expect these interactions to be important at these wavelengths as well. In these  $M = 0$  calculations, the highest harmonics ( $E > I_p$ ) are strongly associated with the  $\text{Ar}^{2+} ^1D$  channels. These channels would not be strongly *disfavored* at 800-nm because of the small energy gap between the  $^3P$  and  $^1D$  thresholds. We would therefore expect the  $^1D$  channels to remain important for HG in  $\text{Ar}^+$  with  $M = 0$  at 800-

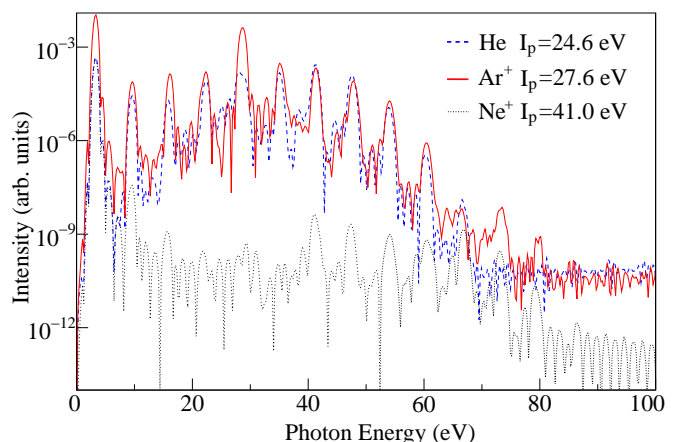


FIG. 4: (Color online) The harmonic spectrum produced by a  $4 \times 10^{14} \text{ Wcm}^{-2}$  390nm laser pulse interacting with  $\text{Ar}^+$  (solid, red line),  $\text{Ne}^+$  (dotted, black line) and He (dashed, blue line). The  $\text{Ne}^+$  spectrum is orders of magnitude lower than the  $\text{Ar}^+$  and He spectra, but the  $\text{Ar}^+$  yield is slightly larger than the He, despite its higher ionization potential.

nm. Hence, application of the three-step model for  $\text{Ar}^+$  with  $M = 0$  should account for multichannel interactions.

The harmonic spectra obtained in the present study demonstrate a significant influence from interference associated with different ionization thresholds. The use of multielectron codes, such as TDRM, is therefore essential for systems with excited thresholds just above the lowest ionization threshold. Atomic systems, such as  $\text{Ar}^+$ , may be suitable for developing understanding of how multichannel interactions affect HG. Further experimental

studies of HG in  $\text{Ar}^+$  would thus be very interesting. We have only addressed the non-relativistic case of  $M = 0$  here, but aim to extend the work to include the effect of  $M = 1$  in our calculations. We also aim to extend these studies to longer wavelengths, which will enable more detailed comparisons with experiment. The recently developed  $R$ -matrix with time-dependence approach [27, 28] will be of major benefit for this extension.

ACB acknowledges support from DEL (NI). HWH is supported by EPSRC under grant number G/055416/1.

- 
- [1] P. Corkum and F. Krausz, *Nat. Phys.* **3**, 381 (2007).
- [2] P. M. Paul, E. S. Toma, P. Breger, G. Mullot, F. Augé, P. Balcou, H. G. Muller, and P. Agostini, *Science* **292**, 1689 (2001).
- [3] S. Baker, J. S. Robinson, C. A. Haworth, H. Teng, R. A. Smith, C. C. Chirilă, M. Lein, J. W. G. Tisch, and J. P. Marangos, *Science* **312**, 424 (2006).
- [4] P. B. Corkum, *Phys. Today* **64**, 36 (2011).
- [5] O. Smirnova, Y. Mairesse, S. Patchkovskii, N. Dudovich, D. Villeneuve, P. B. Corkum, and M. Y. Ivanov, *Nature* **460**, 972 (2009).
- [6] A. D. Shiner, B. E. Schmidt, C. Trallero-Herrero, H. J. Wörner, S. Patchkovskii, P. B. Corkum, J.-C. Kieffer, F. Légaré, and D. Villeneuve, *Nat. Phys.* **7**, 464 (2011).
- [7] A. C. Brown, S. Hutchinson, M. A. Lysaght, and H. W. van der Hart, *Phys. Rev. Lett.* **108**, 063006 (2012).
- [8] P. B. Corkum, *Phys. Rev. Lett.* **71**, 1994 (1993).
- [9] M. Lewenstein, P. Balcou, M. Y. Ivanov, A. L’Huillier, and P. B. Corkum, *Phys. Rev. A* **49**, 2117 (1994).
- [10] S. Pabst, L. Greenman, D. A. Mazziotti, and R. Santra, *Phys. Rev. A* **85**, 023411 (2012).
- [11] M. A. Lysaght, H. W. van der Hart, and P. G. Burke, *Phys. Rev. A* **79**, 053411 (2009).
- [12] A. C. Brown, D. J. Robinson, and H. W. van der Hart, *Phys. Rev. A* **86**, 053420 (2012).
- [13] M. A. Lysaght, P. G. Burke, and H. W. van der Hart, *Phys. Rev. Lett.* **102**, 193001 (2009).
- [14] A. E. Kramida, Y. Ralchenko, J. Reader, and N. A. Team, *Nist atomic spectra database, (ver 5.0)* (2012), URL <http://physics.nist.gov/asd>.
- [15] E. A. Gibson, A. Paul, N. Wagner, R. Tobey, S. Backus, I. P. Christov, M. M. Murnane, and H. C. Kapteyn, *Phys. Rev. Lett.* **92**, 033001 (2004).
- [16] M. Zepf, B. Dromey, M. Landreman, P. Foster, and S. M. Hooker, *Phys. Rev. Lett.* **99**, 143901 (2007).
- [17] A. M. Covington *et al.*, *Phys. Rev. A* **84**, 013413 (2011).
- [18] S. Hutchinson, M. A. Lysaght, and H. W. van der Hart, *J. Phys. B. At. Mol. Opt. Phys.* **43**, 095603 (2010).
- [19] B. Sundaram and P. W. Milonni, *Phys. Rev. A* **41**, 6571 (1990).
- [20] K. Burnett, V. C. Reed, J. Cooper, and P. L. Knight, *Phys. Rev. A* **45**, 3347 (1992).
- [21] J. H. Eberly, Q. Su, and J. Javanainen, *Phys. Rev. Lett.* **62**, 881 (1989).
- [22] G. Bandarage, A. Maquet, T. Ménil, R. Taïeb, V. Vénier, and J. Cooper, *Phys. Rev. A* **46**, 380 (1992).
- [23] J. C. Baggesen and L. B. Madsen, *J. Phys. B. At. Mol. Opt. Phys.* **44**, 115601 (2011).
- [24] D. J. Diestler, *Phys. Rev. A* **78**, 033814 (2008).
- [25] E. S. Smyth, J. S. Parker, and K. Taylor, *Computer Physics Communications* **114**, 1 (1998).
- [26] E. Clementi and C. Roetti, *At. Data Nucl. Data Tables* **14**, 268 (1974).
- [27] L. R. Moore, M. A. Lysaght, L. A. A. Nikolopoulos, J. S. Parker, H. W. van der Hart, and K. T. Taylor, *J. Mod. Optics* **58**, 1132 (2011).
- [28] L. R. Moore, M. A. Lysaght, J. S. Parker, H. W. van der Hart, and K. T. Taylor, *Phys. Rev. A* **84**, 061404 (2011).